Applied Physics Letters

Asymmetric spin dependent scattering at the interfaces of $Si / La_{0.7} Sr_{0.3} M n O_3 / ZnO$ heterostructures

Cite as: Appl. Phys. Lett. **115**, 222401 (2019); https://doi.org/10.1063/1.5115809
Submitted: 20 June 2019 • Accepted: 10 November 2019 • Published Online: 25 November 2019

Bibekananda Das and Prahallad Padhan

Applied Physics Letters ARTICLE scitation.org/journal/apl

Asymmetric spin dependent scattering at the interfaces of Si/$La_{0.7}Sr_{0.3}MnO_3$/ZnO heterostructures

Cite as: Appl. Phys. Lett. **115**, 222401 (2019); doi: 10.1063/1.5115809
Submitted: 20 June 2019 · Accepted: 10 November 2019 ·
Published Online: 25 November 2019

Bibekananda Das and Prahallad Padhan[a)]

AFFILIATIONS

Department of Physics, Indian Institute of Technology Madras, Chennai 600036, India

[a)]padhan@iitm.ac.in

ABSTRACT

A ferromagnetic 120 Å thick $La_{0.7}Sr_{0.3}MnO_3$ (LSMO) film grown on (001)Si using the sputtering deposition technique demonstrates a large positive in-plane magnetoresistance (MR) at 10 K, in the field window of ±0.084 kG to ±0.405 kG, although the bulk LSMO exhibits negative MR. Around the coercive field (∼179 G), the positive MR becomes ∼11%. The positive MR of the LSMO thin film is explained by the charge transfer driven localized strong antiferromagnetic coupling at the Si − LSMO interface, which favors the reduction of the Curie temperature (T_C) of LSMO compared to that of its bulk value. The construction of the interface on the top surface of LSMO with ZnO thin films further reduces T_C ∼ 30 K and the positive MR decreases to ∼1% for 45° oriented in-plane current with the in-plane field. The coupling through Mn − O − Zn at the LSMO − ZnO interface preserves the charge state, and the weak exchange coupling at the (La/Sr)O − ZnO interface reduces the spin-dependent scattering process under the field and thereby, the negative MR. The reduced T_C and in-plane low-field MR at 10 K of a series of Si/LSMO/ZnO are the same irrespective of the ZnO thickness, which confirms their interfacial origin. The presence of interfacial spin disorder at the Si − LSMO interface is further confirmed from the increase in resistance at low temperatures, which is explained by the Kondo like effect and quantum interference effect. Our investigations show that the technologically important interfacial magnetic coupling and magnetoresistance could be achieved and manipulated by the selective interfacial exchange coupling.

The modern information technology sector is largely dependent on Si based metal oxide semiconductor field-effect transistors. There have been several attempts to replace the SiO_2 layer by other oxides with a high K dielectric constant.[1] The use of the Si substrate greatly simplifies the fabrication of microelectromechanical systems based on epitaxial piezoelectric layers[2] and suspended bolometers based on epitaxial $La_{0.7}Sr_{0.3}MnO_3$ (LSMO) thin films.[3] Although the LSMO thin films have been grown on the Si substrate, a perovskite template layer is often used to achieve the epitaxy.[4,5] The direct growth of functional oxides on Si is complicated by the high reactivity of silicon with oxygen and the disruption of epitaxy, which results from the native amorphous SiO_2 layer on the surface of silicon wafers.[4] An additional challenge is a large difference in the thermal expansion coefficients between silicon and these functional oxides: the ratio of thermal expansion coefficients is about a factor of three between room temperature and growth temperature.[4] Recently, we have reported a unique pulsed plasma deposition growth method, where the thin films of LSMO were stabilized epitaxially on a bare Si substrate by using a home-built RF magnetron sputtering technique method.[6]

The strong coupling of spin with charge and orbital degrees of freedom in LSMO has been exploited to manipulate the intriguing physics in the highly stabilized LSMO − ZnO heterostructures.[7–9] The rectifying characteristics,[10] photocarrier injection,[11] ultraviolet photovoltage,[9] and current field modulations[12] have been demonstrated using the current perpendicular to the plane geometry of the LSMO − ZnO interface. In this Letter, we report the study of spin dynamics in LSMO − ZnO for 45° oriented in-plane current with the field. Si/LSMO shows low field positive and high field negative magnetoresistance (MR). However, in Si/LSMO/ZnO, the negative MR range expands, and a very small positive MR is observed under a very low field. This interfacial effect has been explained by using the charge transfer mechanism, the variation of the bond length, and the bond angle at the interfaces.

The highly dense targets of LSMO and ZnO were prepared by using the solid-state reaction method. The detailed processing steps for the synthesis of the LSMO target were presented in a previous report.[6] The high purity ZnO powder was calcined at 900 °C in the air for 24 h and then pelletized at ∼30 kPa in the form of a 2″ diameter disk, followed by sintering at 1200 °C for 24 h. The detailed growth parameters for the deposition of the LSMO thin films on (001) oriented Si were described in a previous article.[6] The thin films of LSMO for this study were deposited at 9×10^{-3} mbar Ar and O_2 gas pressure. After the deposition of LSMO, the ZnO depositions were performed in the pulsed mode at the same growth pressure and temperature of the LSMO by keeping the sputtering power density 5.92 W/cm^2. After the deposition of ZnO, the deposition chamber was filled with 300 mbar O_2 followed by the post-annealing for 45 min, and finally, the films were cooled down to room temperature.

The X-ray diffraction (XRD) patterns and reciprocal space mappings (RSMs) were recorded by using a four-cycle X-ray diffractometer. The temperature and field-dependent in-plane magnetization measurements have been performed by using a superconducting quantum interference device based vibrating sample magnetometer. The field-dependent resistance of the thin films and heterostructures was measured in the two probe configuration by orienting the in-plane current to 45° with respect to the in-plane magnetic field. The transport measurements were carried out using a setup comprised of an Advanced Research System made closed-cycle cryostat, which can be operated from ∼2 K to 400 K, a Lakeshore temperature controller, a Keithley picoammeter, a Keysight nanovoltmeter, and a copper coil solenoid electromagnet with an upper field limit of 1.3 kG.

The $\theta - 2\theta$ XRD patterns of the LSMO thin films grown on a (001) oriented single crystal silicon substrate exhibit only (00l) oriented Bragg's peaks of LSMO and Si.[6] The out-of-plane lattice parameter of the pseudocubic LSMO calculated from its (00l) peak positions of the XRD patterns indicates the presence of ∼−0.28% strain with respect to the bulk LSMO. The growth of the highly oriented pseudocubic perovskite structure of LSMO is realized due to the lattice matching of LSMO along the [110] of Si. Furthermore, the growth of thin films of hexagonal ZnO with different thicknesses on the 120 Å thick pseudocubic LSMO also exhibits only (00l) oriented Bragg's peaks of the constituents and substrate in the XRD patterns [see Fig. 1(a)]. The out-of-plane lattice parameter of ZnO determined from the XRD pattern is 5.21 Å, which is very close to that of its bulk value with a strain of ∼0.08%. The $\theta - 2\theta$ scan of Si/LSMO/ZnO was also performed using the high-resolution monochromator to detect any significant variation of the "c" lattice parameter of ZnO. The high resolution XRD patterns shown in Figs. 1(b) and 1(c) indicate that the c lattice parameter of ZnO in the designed thickness range is relaxed. Furthermore, the reciprocal space mapping (RSM) constructed from Bragg's reflection measurements consisting of $2\theta - \omega$ coupling scans along the [002] of *Si* for different ω values is shown in Fig. 1(d). The in-plane scattering vectors of (002) Si, ZnO and LSMO appear at different reciprocal space parameters, which indicate that Si and LSMO provides fully relaxed growth of LSMO and ZnO, respectively.

The low angle $\theta - 2\theta$ XRD scans of Si/LSMO and Si/LSMO/ZnO are shown in Fig. 1(e). The oscillation period from LSMO is relatively broader and is close to the same value in both Si/LSMO and Si/LSMO/ZnO, which confirms the repeatability of the LSMO thin film growth using the sputtering process. On the other hand, the oscillation period of ZnO in Si/LSMO/ZnO is smaller than that of LSMO and appears before the oscillation of LSMO starts [see Fig. 1(e)]. To determine the film thickness of LSMO and ZnO, the low angle specular x-ray reflectivity was fitted using Philips WINGIXA^{TM} software.[13] The solid line in Fig. 1(e) fitted well to the relative intensity and peak positions of the fringes of the measured XRD patterns. The fit provides the same value of LSMO thickness in both Si/LSMO and Si/LSMO/ZnO, while the thickness of ZnO varies from 372 Å to 930 Å.

The temperature-dependent field-cooled (FC) magnetization [$M(T)$] of 120 Å thick LSMO films grown on Si exhibits paramagnetic-to-ferromagnetic order transition at a temperature (T_C) *of* ∼326 K.[6] The variation of T_C of the perovskite manganite oxide thin films is generally interpreted using Jahn-Teller distortion theory by considering a strain-induced distortion of MnO_6.[14] The T_C of 120 Å thick LSMO film on Si is larger compared to that of $La_{0.75}Sr_{0.25}MnO_3$ grown on $SrTiO_3$ and MgO substrates using RF or DC sputtering.[15] The Si substrate in contact with O_2 forms the Si − O bond, which involves both the covalent and partial ionic characters since the net moment of charge is moved from the silicon valence shell toward that of the oxygen atom.[16] This charge removal results in the oxidation of Si in SiO_2. The difference in the oxidation state dominates the −4 eV shift between the Si − 2p binding energies for Si and SiO_2. The binding energy shift is in general associated with the change in the bond length and bond angle, rehybridization, and the charge transfer. The sp^3 orbitals of Si can either accommodate (La/Sr)O or MnO_2 for the growth of LSMO. The bond lengths of Mn/La/Sr − O are larger than those of Si − O. The change in the valance state of the transition metal modifies the Mn/La/Sr − O bond length; however, the average bond length of Si − O remains unchanged because of the strong covalent

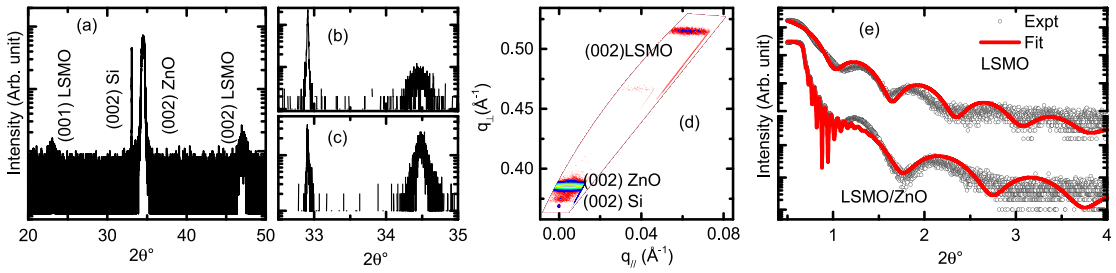

FIG. 1. (a) θ–2θ X-ray diffraction pattern of (001)Si/120 Å $La_{0.7}Sr_{0.3}MnO_3$/930 Å ZnO. High-resolution θ–2θ X-ray diffraction patterns of Si/120 Å LSMO/ZnO with (b) 372 Å and (c) 930 Å thick ZnO. (d) Reciprocal-space-mapping around the (002) of (001)Si/120 Å LSMO/930 Å ZnO. (e) Low angle θ–2θ X-ray diffraction patterns of (001)Si/120 Å LSMO and (001)Si/120 Å LSMO/930 Å ZnO.

bond.[17] Thus, Si leads to the pinning of transition metal ions. In addition, the Si − O − Mn bonding reduced the charge state of Mn.[18] So, the presence of pinned Mn^{3+} near the Si − LSMO interface configured antiferromagnetically ordered spin, which is responsible for the relatively smaller T_C of the LSMO thin film compared to that of its bulk. Nevertheless, the observed T_C, which is closed to that of the bulk LSMO, indicates the presence of perfect stoichiometry in the thin films of $La_{0.7}Sr_{0.3}MnO_3$.[19]

The growth of paramagnetic wurtzite ZnO on the perovskite LSMO introduces the distortion at the interface due to its dissimilar crystal structure and lattice mismatch. The films of LSMO can have (La/Sr)O or MnO_2 termination on the surface, and hence, the ZnO is expected to have two possible interface combinations. For the (La/Sr)O − ZnO interface, the La(5 − *sp*) or Sr(4 − *sp*) energy is considerably lower than the Fermi energy (E_F), and thus, the coupling is weaker between (La/Sr) − *O* − Zn. However, for the MnO_2 − ZnO interface, a strong hybridization between Mn(3*d*) and O(2*sp*) states extends above E_F, and therefore, *O*(2*sp*) is shifted upward, and Zn(4*sp*) is shifted downward.[20] This distortion of O(2*sp*) modulates the hybridization between Mn(3*d*) and O(2*sp*) states, which induces the rotation and tilting of MnO_6. This structural reconstruction at the interface of LSMO − ZnO reduces further the T_C of 120 Å thick LSMO to ∼295 K, irrespective of the ZnO layer thickness [see Fig. 2(b)]. The same value of T_C is observed for all the heterostructures, which indicates that the LSMO thickness is almost equal, and the LSMO − ZnO interface thickness is unchanged for the ZnO thickness range of 372 Å–930 Å. The field-dependent in-plane magnetization [$M(H)$] of these heterostructures measured at 10 K is shown in Figs. 2(c)–2(g). The $M(H)$ of all heterostructures shows hysteresis behavior but does not show any sign of saturation of the magnetization even at 70 kG magnetic field due to the presence of paramagnetic ZnO. The paramagnetic volume increases with the ZnO thickness, and thus, the magnetization of Si/LSMO/ZnO increases with the increase in the ZnO thickness [see Figs. 2(c)–2(g)]. However, the paramagnetic contribution of ZnO in M(H) is negligible for the magnetic field oriented along the [110] and [001] of Si[Fig. 3(a)]. As seen from the lattice mismatch between LSMO and Si,[6] the (100) of LSMO is parallel to the (110) of Si, and thus, the (110) of LSMO is parallel to the (100) of Si [Fig. 3(b)]. The $M(H)$ measured with the field along the [100], [110], and [001] of *Si* indicates that the thin film of LSMO on (001) oriented Si has an easy axis along the [110] of Si [Fig. 3(a)]. Interestingly, the thin film of LSMO on (001) oriented Si exhibits in-plane anisotropy.

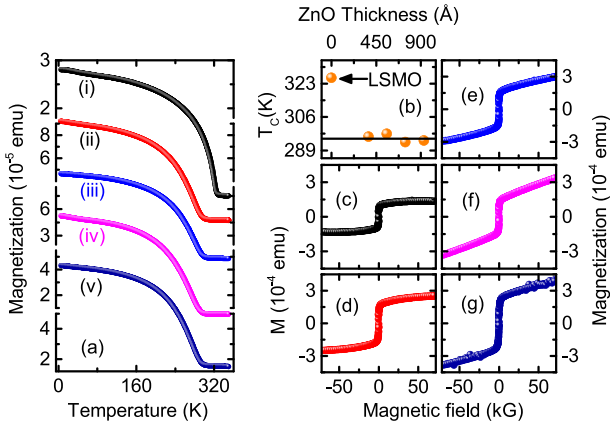

FIG. 2. (a) Temperature dependent 100 G field (along the [100] of Si)-cooled in-plane magnetization of (i) 120 Å thick $La_{0.7}Sr_{0.3}MnO_3$ films and (001)Si/120 Å LSMO/ZnO with (ii) 372 Å, (iii) 558 Å, (iv) 744 Å, and (v) 930 Å thick ZnO. (b) ZnO thickness-dependent T_C. Field dependent in-plane magnetization of (c) 120 Å thick LSMO films and (001)Si/120 Å LSMO/ZnO with (d) 372 Å, (e) 558 Å, (f) 744 Å, and (g) 930 Å thick ZnO.

The resistivity of LSMO films grown on Si, on cooling below 360 K, increases up to 250 K with an anomaly around 326 K, followed by a steady decrease down to 40 K, and then starts increasing gradually down to the lowest temperature. The anomaly in the resistivity corresponds to T_C, while the peak in the resistivity (T_P) is due to the resistivity difference of LSMO [i.e., R_2 in Fig. 4(g)] and the interface of LSMO and Si [i.e., R_1 in Fig. 4(g)]. The rise of resistivity at low temperature ($\lesssim T_{Min} = 40$ K) in the temperature-dependent resistivity $\rho(T)$ has been explained by the quantum correction to the resistivity. The resistivity around T_{min} can be expressed by[21]

$$\rho(T) = \rho_0 + \rho_{\frac{1}{2}} T^{\frac{1}{2}} - \rho_1 \ln(T) + \rho_5 T^5, \quad (1)$$

where $\rho(T)$ is the total resistivity, ρ_0 is the residual resistivity, the second term is due to the contribution of electron-electron scattering, the third term is the spin-dependent Kondo like effect, and the last term is because of the inelastic scattering. The low-temperature $\rho(T)$ [see Fig. 4(a)] has been fitted using Eq. (1). The fit yields $\rho_5 = 6 \times 10^{-13}\,\Omega\,\text{cm}\,\text{K}^{-5}$, which indicates that the contribution to the resistivity of LSMO from the inelastic scattering is negligible. $\rho_{\frac{1}{2}} = 0.003\,\Omega\,\text{cm}\,\text{K}^{-1/2}$ is less than $\rho_1 = 0.009\,\Omega\,\text{cm}$, i.e., the electron-electron scattering is smaller compared to the spin-dependent Kondo like effect, which is consistent with the observed low saturation magnetization of LSMO [see Fig. 2(c)]. The Kondo effect is attributed to the interaction of conduction electrons with the interfacial localized magnetic moment at Si − O − Mn at the interface.

The $\rho(T)$ of Si/LSMO/ZnO is qualitatively similar to that of Si/LSMO with a higher magnitude of resistivity and without any signs of the anomaly in the resistivity around T_C. Apart from the LSMO-ZnO interfacial structural reconstruction, the role of the top-ZnO layer on the absolute value of resistivity is to (i) change the effective resistance of the bilayer, (ii) increase T_{min} due to R_4 [Fig. 4(g)], and (iii) decrease T_P because of R_3 and R_5 [Fig. 4(g)]. The variation of T_{Min} observed in the $\rho(T)$ of Si/LSMO/ZnO with the increase in ZnO layer thickness is negligible, which rules out the significant

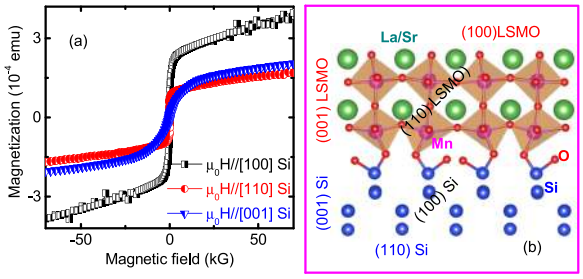

FIG. 3. (a) Field dependent magnetization of (001)Si/120 Å LSMO/ZnO with 930 Å thick ZnO for three different orientations of the magnetic field with respect to Si. (b) Schematic for the growth orientation of LSMO on Si.

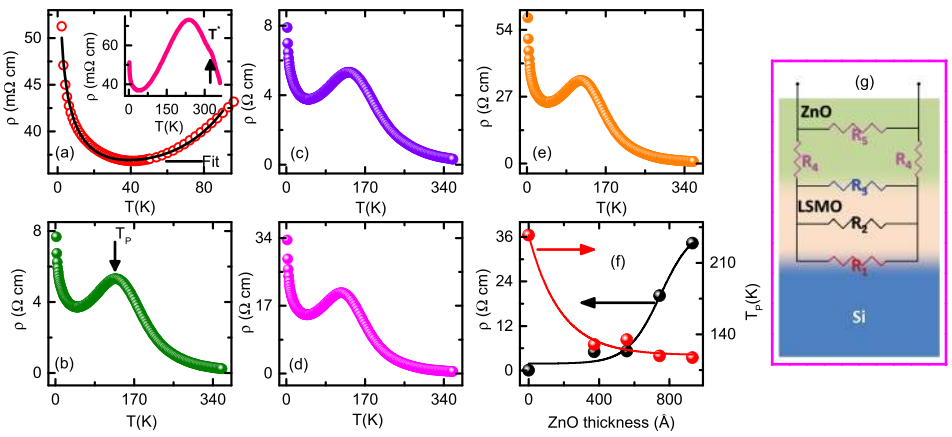

FIG. 4. Temperature-dependent resistivity at low temperatures for (a) (001)Si/120 Å $La_{0.7}Sr_{0.3}MnO_3$. The inset shows its complete temperature-dependent resistivity. Temperature-dependent resistivity of (001)Si/120 Å LSMO/ZnO with (b) 372 Å, (c) 558 Å, (d) 744 Å, and (e) 930 Å thick ZnO. (f) ZnO thickness-dependent resistivity at 10 K and T_p. (g) Sketch of the modeled heterostructure as a combination of series and parallel resistances.

contribution of R_4 [Fig. 4(g)] to the negative temperature coefficient of resistivity for $T < T_{min}$. In Si/LSMO/ZnO, the ZnO layer can be viewed as a combination of in-plane (R_5) and out-of-plane (R_4) resistances, which contribute to the total resistance in parallel and series, respectively. R_5 is so high that the in-plane current in ZnO is negligible, while R_4 increases with the ZnO thickness [see resistivity at 10 K in Fig. 4(f)]. The resistance of LSMO R_2 and its bottom and top interface resistances R_1 and R_3, respectively, contribute to the total resistance in parallel [see the schematic in Fig. 4(g)]. T_P observed in the $\rho(T)$ of Si/LSMO/ZnO is strongly reduced compared to that of Si/LSMO, but a small significant decrease in T_P with the increase in ZnO thickness is observed [see Fig. 4(f)].

The rectangular LSMO strip length on (001) oriented Si is parallel to the [110] of Si [inset of Fig. 5(c)]. However, the maximum magnetic moment with relatively strong pinning is observed along the [100] of Si [Fig. 3(a)]. Thus, the magnetic field is oriented along the [100] of Si (i.e., [110] of LSMO or 45° to in-plane current) for the magnetotransport measurement of the LSMO thin films and LSMO − ZnO bilayer grown on (001) oriented Si. The bulk LSMO is well known for its colossal drops in resistance in the presence of the magnetic field. However, the zero-field resistance of Si/120 Å LSMO is increased in the range of ±0.084 kG to ±0.405 kG field, while it is decreased for the field from 0.084 kG to −0.084 kG and larger than ±0.405 kG. Thus, Si/120 Å LSMO exhibits both negative and positive magnetoresistances ($MR = \frac{R(H)-R(0)}{R(0)} = \frac{\Delta R}{R}$) [see Fig. 5(a)]. The observed positive MR of Si/120 Å LSMO is relatively larger (∼11%) than the positive MR reported for the epitaxial $La_{2/3}Sr_{1/3}MnO_3$ grown on $SrTiO_3$,[22] although a large negative MR, because of the reduced spin disorder at the grain boundary,[23] has been observed in the polycrystalline thin films of $La_{0.67}Sr_{0.33}MnO_3$. However, the large positive MR is scarce and looks counterintuitive since an applied field should reduce magnetic disorder and enhance conductivity. In correlated oxides, the magnetic order in the ground state is expected to be sensitive to electron doping.[24] The electron density increases through the charge transfer[18] via Si − O − Mn, which provides antiferromagnetic order driven by kinetic energy and lower spatial symmetry than the parent structure.[24] The interfacial localized and antiferromagnetically oriented spins with strong coupling contribute resistance R_1, which is responsible for the low field positive MR in Si/LSMO. Interestingly, a maximum positive $MR \sim 1\%$ under a very low field is observed in Si/LSMO/ZnO, and the maximum negative MR is ∼15%. In Si/ LSMO/ZnO, the charge transfer occurring from ZnO to LSMO is very small (∼0.022 e/Å^2),[20] and the oxidation states of La/Sr and Mn are retained during the interface formation and the exchange coupling at (La/Sr)O − ZnO is weak, although the MnO_2 − ZnO interface has strong coupling.[20] Thus, the value of R_3 is

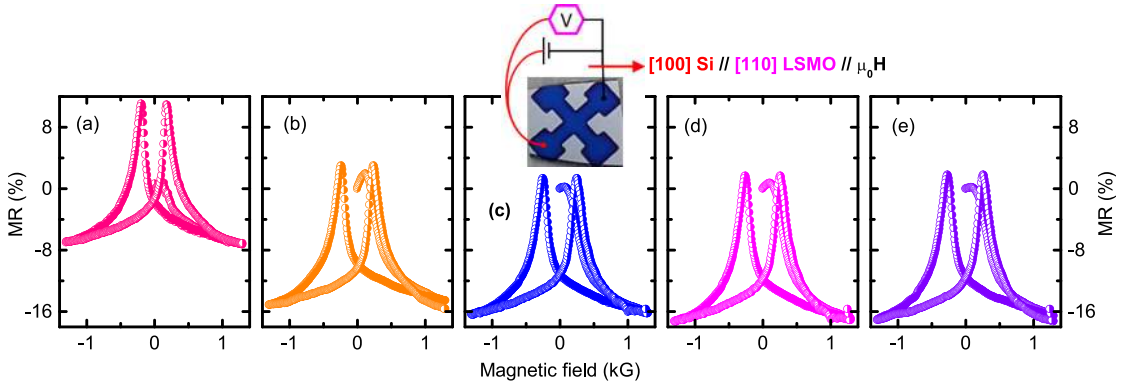

FIG. 5. Field dependent magnetoresistance at 10 K of (a) (001)Si/120 Å $La_{0.7}Sr_{0.3}MnO_3$ and (001)Si/120 Å LSMO/ZnO with (b) 372 Å, (c) 558 Å, (d) 744 Å, and (e) 930 Å thick ZnO. The inset in (c) shows the in-plane current and field orientation.

expected to be closed to that of R_2 and the spin-dependent scattering process is dominated by R_2 and R_3, while R_4 acts as a parasitic contribution to the MR. The MR of LSMO/ZnO is calculated as $(\frac{\Delta R}{R})\%$, where ΔR and R are of the order of $10^6\ \Omega$ for different thicknesses of ZnO, and thus, the total (sum of positive and negative) MR remains more or less the same as that of Si/LSMO ($\sim$16%) eventhough the total resistance of Si/LSMO/ZnO changes dramatically.

In conclusion, a series of $La_{0.7}Sr_{0.3}MnO_3 - ZnO$ heterostructures with 120 Å thick LSMO and different thicknesses of ZnO were grown on (001) oriented Si, using the sputtering process. As anticipated, the same T_C with an increase in the magnetization of Si/LSMO/ZnO is observed for the ZnO layer thickness from 372 Å to 930 Å. Si/120 Å LSMO demonstrates a large positive MR in the field window of ± 0.084 kG to ± 0.405 kG. The positive MR is explained by the charge transfer driven localized strong antiferromagnetic coupling in the $Si - O - Mn$ bond at the interface. The coupling through $Mn - O - Zn$ at the $LSMO - ZnO$ interface preserves the charge state, and the weak exchange coupling at the $(La/Sr)O - ZnO$ reduces the spin-dependent scattering process in the presence of field, which leads to the negative MR. These hosts of the observed positive MR and the change of the MR sign with the selective interface are the intriguing phenomena in modern spintronic based devices, and their tunability could pave the way for innovative technology.

We greatly thank the New Faculty Seed Grant of the Indian Institute of Technology Madras for building the sputtering system. Financial support to set up the transport measurement facility was provided by DAE-BRNS [Project No. 37(3)/14/18/2015]. Thus the authors are thankful to DAE-BRNS and the Principal Collaborator Dr. S. N. Achary.

REFERENCES

[1]N. Setter, D. Damjanovic, L. Eng, G. Fox, S. Gevorgian, S. Hong, A. Kingon, H. Kohlstedt, N. Y. Park, G. B. Stephenson, I. Stolitchnov, A. K. Taganstev, D. V. Taylor, T. Yamada, and S. Streiffer, J. Appl. Phys. **100**, 051606 (2006).
[2]M. D. Nguyen, H. Nazeer, K. Karakaya, S. V. Pham, R. Steenwelle, M. Dekkers, L. Abelmann, D. H. A. Blank, and G. Rijnders, J. Micromech. Microeng. **20**, 085022 (2010).
[3]S. Liu, B. Guillet, A. Aryan, C. Adamo, C. Fur, J.-M. Routoure, F. Lemarié, D. G. Schlom, and L. Méchin, Microelectron. Eng. **111**, 101 (2013).
[4]C. Adamo, L. Méchin, T. Heeg, M. Katz, S. Mercone, B. Guillet, S. Wu, J.-M. Routoure, J. Schubert, W. Zander, R. Misra, P. Schiffer, X. Q. Pan, and D. G. Schlom, APL Mater. **3**, 062504 (2015).
[5]Z. Trajanovic, C. Kwon, M. C. Robson, K.-C. Kim, M. Rajeswari, R. Ramesh, T. Venkatesan, S. E. Lofland, S. M. Bhagat, and D. Fork, Appl. Phys. Lett. **69**, 1005 (1996).
[6]P. Padhan, U. K. Sinha, and A. Sahoo, Rev. Sci. Instrum. **89**, 085102 (2018).
[7]Y. Feng and M. Zhang, J. Magn. Magn. Mater. **322**, 2675 (2010).
[8]S. Chattopadhyay, J. Panda, and T. K. Nath, J. Appl. Phys. **113**, 194501 (2013).
[9]K. X. Jin, S. G. Zhao, C. L. Chen, X. Y. Tan, and X. W. Jia, J. Phys. D **42**, 015001 (2009).
[10]A. Tiwari, C. Jin, D. Kumar, and J. Narayan, Appl. Phys. Lett. **83**, 1773 (2003).
[11]K. Lord, D. Hunter, T. M. Williams, and A. K. Pradhan, Appl. Phys. Lett. **89**, 052116 (2006).
[12]P. S. Solanki, U. Khachar, M. Vagadia, A. Ravalia, S. Katba, and D. G. Kuberkar, J. Appl. Phys. **117**, 145306 (2015).
[13]A. V. Ravindra, P. Padhan, and W. Prellier, Appl. Phys. Lett. **101**, 161902 (2012).
[14]A. J. Millis, T. Darling, and A. Migliori, J. Appl. Phys. **83**, 1588 (1998).
[15]P. M. Leufke, A. K. Mishra, A. Beck, D. Wang, C. Kübel, R. Kruk, and H. Hahn, Thin Solid Films **520**, 5521 (2012).
[16]R. F. Stewart, M. A. Whitehead, and G. Donnay, Am. Mineral. **65**, 324 (1980).
[17]G. Zhong, Y. Li, P. Yan, Z. Liu, M. Xie, and H. Lin, J. Phys. Chem. C **114**, 3693 (2010).
[18]D. W. Kim, S. Uchida, H. Shiiba, N. Zettsu, and K. Teshima, Sci. Rep. **8**, 11771 (2018).
[19]Å. Monsen, J. E. Boschker, F. Macià, J. W. Wells, P. Nordblad, A. D. Kent, R. Mathieu, T. Tybell, and E. Wahlström, J. Magn. Magn. Mater. **369**, 197 (2014).
[20]A. Mahmoud, L. Maschio, M. F. Sgroi, D. Pullini, and A. M. Ferrari, J. Phys. Chem. C **121**, 25333 (2017).
[21]W. Niu, M. Gao, X. Wang, F. Song, J. Du, X. Wang, Y. Xu, and R. Zhang, Sci. Rep. **6**, 26081 (2016).
[22]S. P. Chiu, M. Yamanouchi, T. Oyamada, H. Ohta, and J. J. Lin, Phys. Rev. B **96**, 085143 (2017).
[23]X. W. Li, A. Gupta, G. Xiao, and G. Q. Gong, Appl. Phys. Lett. **71**, 1124 (1997).
[24]P. Sanyal, H. Das, and T. Saha-Dasgupta, Phys. Rev. B **80**, 224412 (2009).